Robust high-dynamic-range optical roll sensing

Steven R. Gillmer,1,* Xiangzhi Yu,1 Chen Wang,2 and Jonathan D. Ellis1,3

¹Department of Mechanical Engineering, University of Rochester, Rochester, New York 14627, USA
²Department of Electrical and Computer Engineering, University of Rochester, Rochester, New York 14627, USA
³The Institute of Optics, University of Rochester, Rochester, New York 14627, USA
*Corresponding author: steven.gillmer@rochester.edu

Received March 23, 2015; revised April 28, 2015; accepted May 3, 2015; posted May 5, 2015 (Doc. ID 236525); published May 20, 2015

We present a robust optical-roll sensor with a high-dynamic range and high-throughput capabilities. The working principle relies on tracking the amplitude of an optical square wave-encoded light source. After encoding a square wave onto a polarization reference, quadrature demodulation of the polarized light allows us to cancel common-mode noise. Benefits of this sensor include its simplicity, low cost, high-throughput, insensitivity to source amplitude fluctuations, and no inherent drift. In this Letter, we present the working principle and experimentally validate a 43° usable working range with 0.002° resolution. This sensor has the highest reported dynamic range for optical roll sensing. © 2015 Optical Society of America

OCIS codes: (120.0120) Instrumentation, measurement, and metrology; (120.3930) Metrological instrumentation; (120.4640) Optical instruments; (230.5440) Polarization-selective devices.

http://dx.doi.org/10.1364/OL.40.002497

Out of the six degrees of freedom between any two systems, the roll angle has classically been the hardest to measure using optical methods. Angular-roll sensors play an invaluable role in general robotics and instrumentation [1], the calibration of coordinate measurement machines (CMMs) and computer numerically controlled (CNC) manufacturing equipment [2,3], and the automated rendezvous and docking between spacecraft [4,5]. Regardless of the application, an inherent trade-off between range and resolution exists in the development of current optical-roll sensors. In the calibration of CMMs and CNC machines, for example, high-resolution sensors have been realized at the cost of measurement range [6-13]. In contrast, Li et al. presented a compact and robust roll-angle sensor with a notably large dynamic range [14]. Their sensor relies on a Faraday polarization rotator that alternately rotates linear polarization about a fixed analyzer to create an optical square wave-encoded output. Based on the amplitude of the square wave, the roll about the fixed polarization analyzer can be extracted. Their sensor is low-cost, compact, flexible, and insensitive to amplitude fluctuations as long as they are slower than one optical cycle of the Faraday rotator. Unfortunately, to measure the roll angle using their sensor, they require amplitude measurement of a differential signal output from a single photodetector, a task that is not necessarily straightforward and requires specialized electronics to achieve.

In this Letter, we realize a low-cost, high-throughput roll-angle sensor with straightforward operation and increased resolution compared to previous work by Li et al. Instead of using a Faraday rotator, our signal is encoded using an acousto-optic modulator (AOM), our roll sensing element is a half-wave plate, and we implement a polarizing beamsplitter (PBS) to create a quadrature output of the signal amplitude. Our novel sensor can be readily implemented in a high-throughput application with no signal drift over long-term measurements with high accuracy. Furthermore, our adaptations have the following advantages. First, by creating a quadrature

output using a PBS, we improve the resolution by $5\times$ (0.01° to 0.002°). Second, this method uses two detectors that carry reference-single-ended (RSE) signals. The two signals can now be demodulated efficiently and in a straightforward manner using methods such as lock-in detection or the single-bin discrete Fourier transform algorithms [15]. These two methods have become increasingly standardized for high-resolution and highbandwidth amplitude demodulation. Third, our quadrature detection creates highly efficient common-mode noise rejection. It was previously necessary for amplitude fluctuations, temperature changes, and vibrations to occur at a rate slower than one optical cycle of the carrier signal to achieve insensitive roll measurements to these effects [14]. In the present configuration, this limitation is removed. All common-mode noise will appear in both D.C. output signals $(V_1 \text{ and } V_2 \text{ in Fig. } \underline{1})$ and is canceled using Eq. (8). The primary advantage of this adaptation is the driving signal can be pushed to higher frequencies, thereby reducing 1/f noise in the measurement electronics. At the time of this publication,

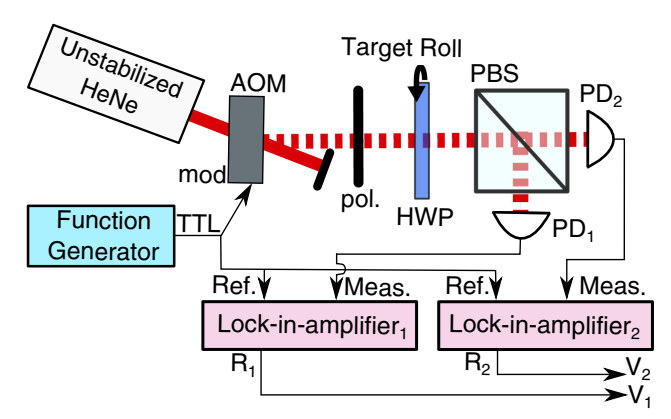


Fig. 1. Full schematic of the compact roll sensor. V_1 and V_2 are post-processed to extract roll using Eq. (8).

our new approach represents the largest reported dynamic range in optical roll sensing.

A schematic of our roll-angle sensor is shown in Fig. 1. We adopted a 12-mW unstabilized Helium-Neon laser source that could be replaced by a laser diode or other semi-coherent optical device. The beam is passed through an acousto-optic modulator that modulates the first diffracted order according to the modulation TTL (transistor-transistor logic) input from a function generator. Our function generator signal is split and used as the reference signal for the two lock-in amplifiers. The modulated optical signal passes through a polarizer and half-wave plate that rotates the polarization reference twice the roll angle. As a response to HWP roll, the PBS selects horizontal and vertical components of our rotated polarization and thus, as one photodetector records an increase in optical intensity, the other records a decrease. The raw square wave signals from each photodetector are sent to the measurement channels of two separate lock-in amplifiers that process the data in real time using parallelized lock-in detection.

The optical square wave at the output of the AOM is represented by its time domain Fourier series expansion,

$$Z_{\text{sqr}}(t) = \frac{4}{\pi} \sum_{n=1}^{\infty} \frac{\sin(2\pi(2n-1)ft)}{(2n-1)},$$
 (1)

where f is the fundamental driving frequency, and t is time. In the limit of $n \to \infty$, this expression represents a perfect square wave. For discrete summations of n, it can be seen that our signal is a summation of odd sine harmonics with decreasing amplitude. For the results presented in this Letter, we have set our driving frequency at 50 kHz, thus the second harmonic of the square wave is 150 kHz. We set the time constant on our lockin-amplifiers to 3 ms, which represents a nominal 53-Hz first low-pass filter using lock-in detection [15]. As a result, we are only measuring the first harmonic of the square wave. We chose to drive the modulation input of the AOM using a TTL signal for similar reasons to those discussed by Li et al. [14]. In their manuscript, they discuss the possibility of driving their Faraday rotator with a pure sine wave instead of running the rotator in saturation, which produces an optical square wave. In this fashion, if the temperature changes, so does the Verdet constant of the Faraday rotator. Feedback compensation can be implemented but at an unnecessary cost of complexity. Li et al. instead drove their Faraday rotator in saturation, thereby stabilizing their carrier square wave signal. We have noticed a similar effect with our AOM. If we drive the modulation with a sine wave, nonlinearities in the AOM produce an unstable sine wave modulation output. Instead, we drive our AOM in saturation; this is accomplished using a digital AOM driver (Isomet 522C-x Series). In saturation, the optical square wave output amplitude is inherently stable. Furthermore, analog-to-digital converters in our lock-in amplifiers benefit from detecting the easily discernable rising edge of our carrier signal.

The Jones matrices for all elements in our system are represented by

$$\mathbf{P_1} = \begin{bmatrix} 1 & 0 \\ 0 & 0 \end{bmatrix}$$

$$\mathbf{P_2} = \begin{bmatrix} 0 & 0 \\ 0 & 1 \end{bmatrix}$$

$$\mathbf{H}(\alpha) = \begin{bmatrix} \cos(2\alpha) & -\sin(2\alpha) \\ \sin(2\alpha) & -\cos(2\alpha) \end{bmatrix}$$

$$\mathbf{E_i} = \begin{bmatrix} 0 \\ A_i Z_{\text{sqr}}(t) \end{bmatrix}, \tag{2}$$

where \mathbf{P}_1 and \mathbf{P}_2 in Eq. (2) represent the horizontal or vertical selections of the PBS toward photodetectors 1 and 2, respectively, $\mathbf{H}(\alpha)$ is the half-wave plate that is oriented at the angle α , A_i is the initial amplitude of the optical square wave at the output of the AOM, $Z_{\rm sqr}(t)$ is defined in Eq. (1), and thus $\mathbf{E}_{\rm i}$ defines the polarization reference for our roll sensor after passing through the initial linear polarizer. To analyze the signal at both photodetectors we propagate the input signal according to

$$\mathbf{E}_{\mathbf{s},\mathbf{j}} = \mathbf{P}_{\mathbf{j}}\mathbf{H}(\alpha)\mathbf{E}_{\mathbf{i}},\tag{3}$$

where the subscript j is used to designate either arm of the PBS. The output $\mathbf{E_{s,j}}$ can be shown to be equal to the quadrature signals

$$\mathbf{E_{s,1}} = \begin{bmatrix} -A_i \sin(2\alpha) Z_{\text{sqr}}(t) \\ 0 \end{bmatrix}$$

$$\mathbf{E_{s,2}} = \begin{bmatrix} 0 \\ -A_i \cos(2\alpha) Z_{\text{sqr}}(t) \end{bmatrix}.$$
(4)

Figure $\underline{2}$ demonstrates this concept further. We drove the modulation input of the AOM with a 1-kHz TTL signal and recorded the raw voltages at the output of photodetectors 1 and 2. In a response to, e.g., 10-degree rotation of the HWP, the raw voltage output increases or decreases by nominally 1.25 V in our setup depending on horizontal or vertical polarization selection through the PBS.

To calculate roll angle using Eq. (4), we analyze optical intensity as the modulus squared:

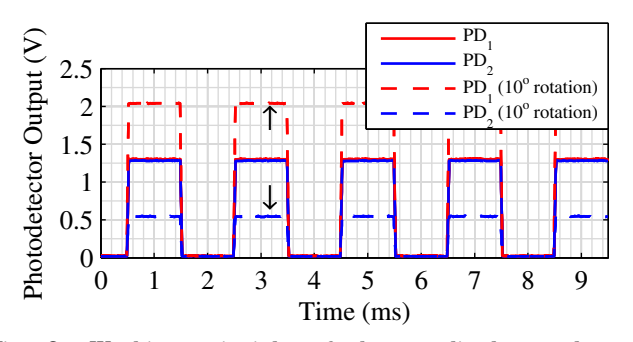


Fig. 2. Working principle of the amplitude quadrature demodulation using a PBS as a polarization analyzer. The raw voltages are recorded at the output of photodetectors 1 and 2.

$$\begin{split} I_{s,1} &= A_i^2 \sin^2(2\alpha) Z_{\text{sqr}}^2(t) \\ I_{s,2} &= A_i^2 \cos^2(2\alpha) Z_{\text{sqr}}^2(t), \end{split} \tag{5}$$

and thus photodetector output voltages are defined by

$$\begin{aligned} & \text{PD}_{1} \propto A_{i}^{2} \sin^{2}(2\alpha) Z_{\text{sqr}}^{2}(t) \\ & \text{PD}_{2} \propto A_{i}^{2} \cos^{2}(2\alpha) Z_{\text{sqr}}^{2}(t). \end{aligned} \tag{6}$$

It is convenient to assume the photodetectors are initially balanced, which occurs when the HWP is set to $\alpha_0=22.5^\circ$, then the two expressions from Eq. (6) are set equal to each other using their common variables, $A_s^2Z_{\rm sor}^2(t)$, according to

$$\frac{V_1}{\cos^2[2(\alpha_0 - \alpha_r)]} = \frac{V_2}{\sin^2[2(\alpha_0 - \alpha_r)]}.$$
 (7)

In Eq. (7) the signals PD₁ and PD₂ have been passed through two separate lock-in amplifiers to extract their amplitude change. The amplitude (R_j) output from each lock-in amplifier can be defined in terms of volts, V_1 and V_2 . Furthermore, we note that from the initial balanced case in which $\alpha_0 = 22.5^\circ$, the change in roll is defined as α_r . Using the identities $2\sin^2(\theta) = 1 - \cos(2\theta)$ and $2\cos^2(\theta) = 1 + \cos(2\theta)$, it is straightforward to show that $V_1(1 - \cos(90^\circ - 4\alpha_r)) = V_2(1 + \cos(90^\circ - 4\alpha_r))$, which is equivalent to $V_1(1 - \sin(4\alpha_r)) = V_2(1 + \sin(4\alpha_r))$. Finally, roll is extracted using

$$\alpha_r = \frac{\arcsin\left(\frac{V_1 - V_2}{V_1 + V_2}\right)}{4}.\tag{8}$$

In practice, our HWP is imperfect. To achieve all results presented in this manuscript we have calibrated the retardance of the waveplate as $\lambda/1.939$. Therefore our post processing algorithm for all presented experimental

results is $\alpha_{\text{calibrated}} = \frac{\arcsin(\frac{V_1 - V_2}{V_1 + V_2})}{(2*1.939)}$. For high accuracy, this calibration is critical.

The performance of the PBS is of particular interest as well because some cubes possess a high extinction ratio in one arm compared to the other. Our PBS was purchased from Thorlabs (model PBS251) with a specified extinction ratio of >1000:1. If a PBS with unequal polarization separation is used, it will not affect the accuracy of roll displacement measurements. It will, however, provide a slight offset of the zero value of the sensor which would limit the range in one direction.

To qualify the accuracy of this sensor, we compare its rotational readout to a measured pitch using the industry standardized Renishaw XL-80 Laser Measurement System. Our HWP and Renishaw's differential retroreflectors are rigidly mounted together to ensure the measurement of the orientation of a single artifact. The XL-80 measures pitch from the orthogonal direction compared to our roll sensor. We cannot compare our roll readings to a Renishaw roll reading since that calibration does not exist for the system we used. We analyzed rotation using the NewFocus Motorized Five-Axis Tilt Aligner by Newport. The results are plotted in Fig. 3, and have been

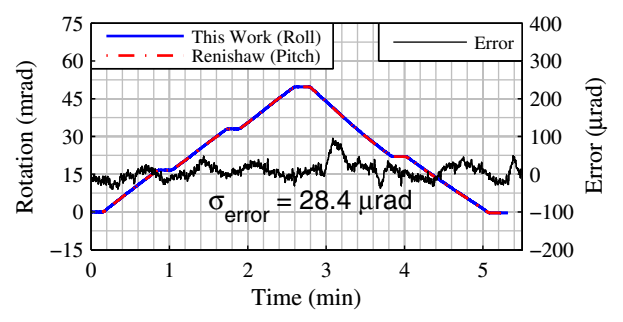


Fig. 3. Results of a long-range qualification experiment between our roll sensor and the Renishaw XL-80 Laser Measurement System. The standard deviation of the error was $28.4~\mu rad~(0.0016^\circ)$ over a 50-mrad range.

subjected to a final 200-Hz low-pass filter to reduce the influence of noise. The standard deviation of the error is $28.4 \mu rad (0.0016^{\circ})$ over a 50-mrad range.

This sensor has a resolution of $40~\mu rad~(0.0023^\circ)$ over a usable range of $0.75~rad~(43^\circ)$. Theoretically, we should be able to measure roll within a full 45° range according to Eq. (8). In practice, however, this is reduced slightly because the PBS is imperfect, and some unintended light will always leak through the horizontal and vertical analyzer. To experimentally validate the full range we could not use the NewFocus Motorized Five-Axis Tilt Aligner or compare our results to the Renishaw XL-80 Laser Measurement System as both have a range on the order of single degrees. Our full range is examined in Fig. 4.

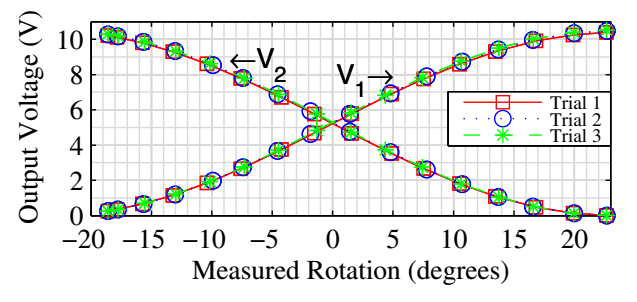


Fig. 4. Validation of the full usable working range of this roll sensor. The theoretical working range is 45° , however, the usable working range is a reduced 43° due to an imperfect polarizing beamsplitter.

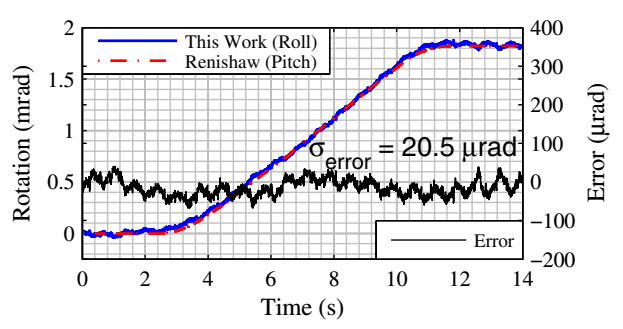


Fig. 5. To examine repeatability, the standard deviation of the error after eight consecutive trials of this representative measurement is tabulated in Table 1.

Table 1. Standard Deviations of the Sensor Error over Eight Consecutive Trials^a

Trial	1	2	3	4	5	6	7	8
Std. Dev. (µrad)	24.9	17.6	26.4	13.3	16.5	16.6	20.5	17.4

^aA representative measurement for these trials is plotted in Fig. 5.

The full range was validated using a HWP rotation mount that was rotated by hand in nominal 3-degree increments. Each data point is the result of a 750-point average sampled from the lock-in amplifiers to our host PC at 500 Hz. Figure $\underline{4}$ plots the output voltages from both lock-in amplifiers in addition to the measured roll angle calculated using a calibrated Eq. (8). The authors note this same experiment was performed by Li $et~al.~[\underline{14}]$ for comparison to their sensor.

To examine the repeatability of our roll measurements, we carried out eight successive roll/pitch qualifications with a representative measurement shown in Fig. 5. The standard deviation is noted on that figure, and the standard deviations over all eight measurements are tabulated in Table 1. It is evident that our discussed sensor has a high level of repeatability over eight trials. Furthermore, the standard deviations of the errors are consistently below the resolution of the sensor.

To summarize, we have presented a robust optical roll sensor with the largest reported dynamic range to date. After a calibration of the exact retardance of the target HWP, this sensor can reliably measure target roll with a resolution of 0.002° in a 43° usable working range. Standard deviations of the error when compared to the Renishaw XL-80 Laser Measurement System are consistently below the resolution of the sensor demonstrating high accuracy. Due to its simplicity and high-throughput capabilities, our sensor can be readily implemented with straightforward operation.

We would like to thank Dr. Shane Woody and Dr. Tieli Zhang for fruitful discussions regarding this research.

This work was funded in part by the National Science Foundation under awards CMMI:1265824 and STTR:1417032 and the US Department of Commerce, National Institute of Standards and Technology under Award No. 70NANB12H186.

References

- P. P. Regtien, Sensors for Mechatronics (Elsevier, 2012), pp. 161–217.
- C. Lee, G. H. Kim, and S.-K. Lee, Meas. Sci. Technol. 22, 105901 (2011).
- 3. S. W. Lee, R. Mayor, and J. Ni, J. Manuf. Sci. Eng. **127**, 857 (2005)
- 4. K.-H. Kolk and B. G. Moebius, Proc. SPIE 4134, 290 (2000).
- E. Tanner, S. Granade, and C. A. Whitehead, Proc. SPIE 5086, 329 (2003).
- Z. Liu, D. Lin, H. Jiang, and C. Yin, Sens. Actuators A 104, 127 (2003).
- C.-M. Wu and Y.-T. Chuang, Sens. Actuators A 116, 145 (2004).
- Y. Zhai, Q. Feng, and B. Zhang, Opt. Laser Technol. 44, 839 (2012).
- W. Chen, S. Zhang, and X. Long, Opt. Express 21, 8044 (2013).
- 10. Y. Le, W. Hou, K. Hu, and K. Shi, Opt. Lett. 38, 3600 (2013).
- 11. F. Qibo, Z. Bin, C. Cunxing, K. Cuifang, Z. Yusheng, and Y. Fenglin, Opt. Express 21, 25805 (2013).
- 12. H.-L. Hsieh and S.-W. Pan, Opt. Express 23, 2451 (2015).
- 13. "XD6 Precision Laser Measurement System," http://www.apisensor.com/index.php/products-en/machine-tool-calibration-en/xd-laser-en (cited March 2015).
- 14. S. Li, C. Yang, E. Zhang, and G. Jin, Opt. Lett. 30, 242 (2005).
- 15. J. D. Ellis, Field Guide to Displacement Measuring Interferometry (SPIE, 2014).